Letter

Electronic correlations and superconducting instability in $La_3Ni_2O_7$ under high pressure

Frank Lechermann, Jannik Gondolf, Steffen Bötzel, and Ilya M. Eremin
Institut für Theoretische Physik III, Ruhr-Universität Bochum, D-44780 Bochum, Germany

(Received 13 June 2023; revised 2 October 2023; accepted 16 November 2023; published 30 November 2023)

Motivated by the report of superconductivity in bilayer $La_3Ni_2O_7$ at high pressure, we examine the interacting electrons in this system. First-principles many-body theory is utilized to study the normal-state electronic properties. Below 100 K, a multiorbital non-Fermi-liquid state resulting from a loss of Ni-ligand coherence within a flat-band-dominated low-energy landscape is uncovered. The incoherent low-temperature Fermi surface displays strong mixing between Ni-d_{z^2} and Ni-$d_{x^2-y^2}$ orbital character. In a model Hamiltonian picture, spin fluctuations originating mostly from the Ni-d_{z^2} orbital give rise to strong tendencies towards a superconducting instability with a B_{1g} or B_{2g} order parameter. The dramatic enhancement of T_c in pressurized $La_3Ni_2O_7$ is due to stronger Ni-d_{z^2} correlations compared to those in the infinite-layer nickelates.

DOI: 10.1103/PhysRevB.108.L201121

Introduction. In a recent finding, Sun *et al.* [1] reported superconductivity near a temperature $T = 80$ K in bulk single-crystalline $La_3Ni_2O_7$ at pressures $p > 14$ GPa. This adds a whole new chapter to the young research field of superconducting (SC) nickelates, hosting high-T_c cuprate-akin NiO_2 square-lattice planes. The field has been inaugurated by the discovery of electron pairing in thin films of Sr-doped infinite-layer $NdNiO_2$ with a $T_c \sim 15$ K in 2019 [2]. Early follow-up studies [2–8] detected similar SC phases in thin films of $Pr_{1-x}Sr_xNiO_2$, $La_{1-x}Sr_xNiO_2$, and also in multilayer $Nd_6Ni_5O_{12}$ thin films. While these reduced SC nickelates share a common motif by the lack of apical oxygens (resulting from a topotactic reaction) and Ni($3d^{9-\delta}$) oxidation states, the characteristics of bilayer $La_3Ni_2O_7$ differ. It still holds the apical oxygens and Ni formally has a $3d^{7.5}$ configuration. Furthermore, a comparison to high-T_c cuprates with their key Cu-$d_{x^2-y^2}$ single-orbital character becomes quite stretched. Whereas there is an ongoing debate concerning a dominant single Ni-$d_{x^2-y^2}$ [9–20] versus dominant multiorbital Ni-e_g [21–25] low-energy physics in reduced SC nickelates, the nominal hole doping away from Ni($3d^9$) is that large in $La_3Ni_2O_7$ as to render Ni multiorbital physics inevitable. In this context, a Ni-e_g multiorbital picture for infinite-layer nickelates results in a competition between SC instabilities of varying flavor [26].

On a wider scope, two further issues appear relevant. First, even if the formal oxidation state reads accordingly, a Ni($3d$) occupation well below $n_d = 8$ is hardly occurring in known nickel oxides. Instead, in most cases, a $3d^8\underline{L}$ state incorporating holes on ligand oxygen is realized [27–33], also accompanied by a smaller charge-transfer energy $\Delta = \varepsilon_d - \varepsilon_p$ between Ni($3d$) and O($2p$). Second, bilayer oxides from the p-layered Ruddlesden-Popper series $A_{p+1}TM_pO_{3p+1}$ (A: rare-earth, alkaline-earth; TM: transition metal) often display a much more delicate normal-state low-energy physics than corresponding single-laver systems. This is, e.g., exemplified for ruthenates [34–36] and iridates [37]. Previous theoretical accounts of bilayer lanthanum nickelate focused on the paramagnetic metal [38–40] at ambient pressure. From density-functional theory (DFT), a charge-density-wave state was predicted [41], while DFT+Hubbard U considerations [42] remark the possible relevance of magnetically ordered states.

In this Letter, we provide a theoretical description of the correlated electronic structure of paramagnetic $La_3Ni_2O_7$ under high pressure, by employing a combination of DFT, self-interaction correction (SIC), and dynamical mean-field theory (DMFT), i.e., the so-called DFT+sicDMFT approach [43]. Moreover, a model Hamiltonian perspective via the random-phase approximation (RPA) onto the possible superconducting instabilities from spin fluctuations is presented. We reveal an intriguing low-energy physics of pressurized $La_3Ni_2O_7$ in the normal state. The highly correlated interplay between Ni-d_{z^2}, Ni-$d_{x^2-y^2}$, and O($2p$), with the former displaying a partial flat-band character, gives rise to a distinct non-Fermi-liquid (NFL) regime below $T < 100$ K. The model RPA investigation points to a B_{1g} or B_{2g} SC order parameter that would emerge from this multiorbital scenario. Most importantly, we argue that the Ni-d_{z^2} orbital is much more correlated in the bilayer case than in infinite-layer nickelates. Consequently, it interacts in a much more concerted fashion with Ni-$d_{x^2-y^2}$, which could explain the much higher T_c in the bilayer case. Note that Ni-$d_{x^2-y^2}$ is always close to half filling in superconducting nickelates and alone cannot explain the difference in T_c between these two classes of materials.

Theoretical approach. The charge self-consistent [44] DFT+sicDMFT framework [43], where the Ni sites act as DMFT impurities and Coulomb interactions on oxygen enter by SIC on the pseudopotential level [45], is put into practice. The DFT part consists of a mixed-basis pseudopotential code [46–48] and SIC is applied to the O($2s, 2p$) orbitals via weight factors w_p. While the $2s$ orbital is fully corrected with $w_p = 1.0$, the choice [22,43,45] $w_p = 0.8$ is used for $2p$ orbitals. Continuous-time quantum Monte Carlo in hybridization expansion [49] as implemented in the TRIQS code [50,51] solves the DMFT problem. A five-orbital general Slater-Hamiltonian, parametrized by Hubbard $U = 10$ eV and

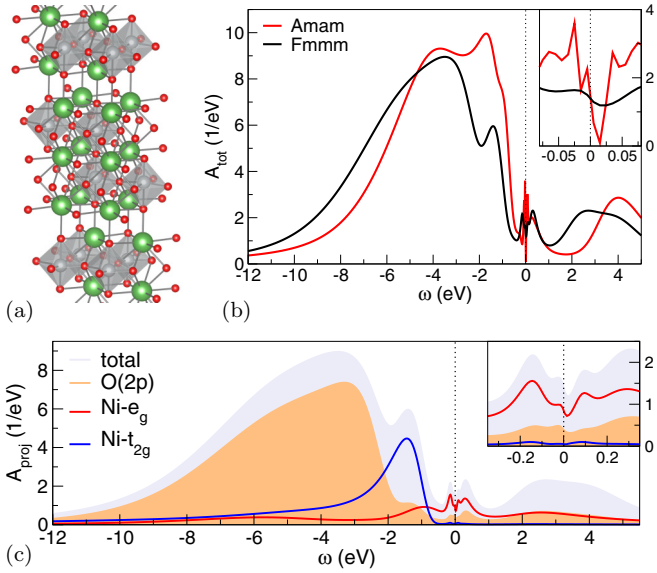

FIG. 1. **k**-integrated electronic spectrum from DFT+sicDMFT at $T = 80$ K. (a) $Fmmm$ crystal structure of $La_3Ni_2O_7$ with the c axis vertical: La (green), Ni (gray), and O (red). Note the bilayer of edge-sharing NiO_6 octahedra in the center and along c, bounded by LaO_2 layers up and below. (b) Total spectral function of low-pressure $Amam$ and high-pressure $Fmmm$ phase (inset: low-energy blowup). (c) Site- and orbital-projected spectral function for the $Fmmm$ phase (inset: low-energy blowup).

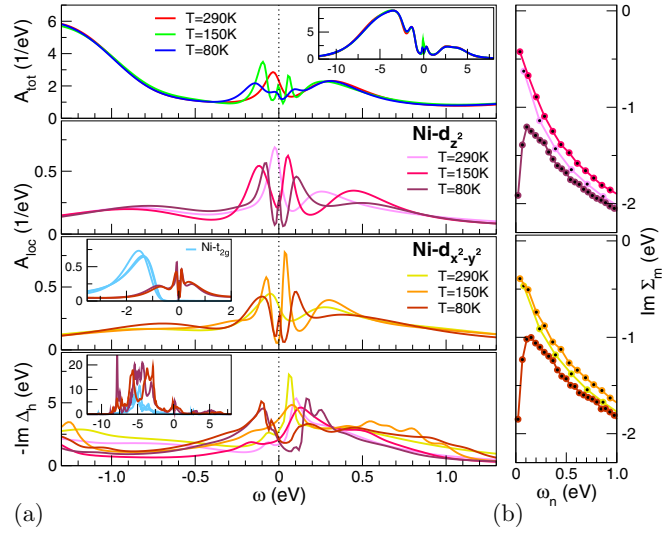

FIG. 2. FL-like vs NFL behavior with T in the $Fmmm$ phase from DFT+sicDMFT. (a) Top panel: Total spectral function (inset: wide energy scale). Middle panels: Local Ni-e_g spectral function (inset: wide energy scale including local Ni-t_{2g} spectra for $T = 80$ K). Bottom panel: Ni-e_g hybridization function (inset: same protocol as for middle panels). (b) Imaginary part of the Ni-e_g self-energies $\Sigma(i\omega_n)$ on the Matsubara axis [colors according to the middle panel of (a)].

Hund exchange $J_H = 1$ eV [22,23], governs the correlated subspace defined by Ni(3d) projected local orbitals [52]. Crystallographic data are taken from experiment [1]. Further calculational details are given in the Supplemental Material [53] (with Refs. [54–61]).

Results. In experiment, there is a structural transition in $La_3Ni_2O_7$ from a low-pressure *Amam* phase with finite NiO_6 octahedral tilting to a high-pressure $Fmmm$ phase without tilting [1]. The *Amam* (space group No. 63) crystal structure has four equivalent Ni sites in the primitive cell, in contrast to two Ni sites for the $Fmmm$ (space group No. 69) one. The key feature of the latter structure at $p = 29.5$ GPa [see Fig. 1(a)] is a rather small distance of $\sim$1.76 Å between Ni and apical oxygen within the bilayer. The calculations show [cf. Fig. 1(b)] that the spectrum of the *Amam* phase at $p =$ 1.6 GPa is (nearly) gapped, in line with the measured different transport properties [1]. For the rest of this Letter, we will restrict the discussion to the properties of the high-pressure $Fmmm$ phase.

The electronic spectrum in Fig. 1(c) exhibits a metallic state with Ni-e_g $\{d_{z^2}, d_{x^2-y^2}\}$ and O($2p$) character at the Fermi level ε_F, but lacks a strong quasiparticle (QP) signature. The Ni-t_{2g} $\{d_{xz}, d_{yz}, d_{xy}\}$ manifold is mostly filled with a peak at ~ -1.5 eV. The main O($2p$) weight peaks at ~ -3.5 eV. Sizable O($2p$) weight in the unoccupied part of the spectrum points to ligand-hole states. And indeed, the integrated projected spectral parts yield occupations $n_d = 7.98$ and $n_p =$ 5.60, resulting in a substantial content of 0.4 holes per oxygen and a near Ni($3d^8$) configuration. Thus maybe unsurprisingly for this high-pressure system, the degree of covalency is significant and about 1.8 formula-unit-cell valence electrons have to reside in states of La($5d6s$) and/or Ni($4s$) character. The DFT+sic computed charge-transfer energy $\Delta = 3.6$ eV lies in between the infinite-layer values of 5.0 eV for $NdNiO_2$ and of 1.3 eV for $SrCuO_2$ [22]. Note in this respect that while the Ni-e_g character dominates at ε_F, the corresponding O($2p$) content is still larger than in $NdNiO_2$, hinting to a comparatively enhanced role of oxygen degrees of freedom at low energy.

As anticipated for a bilayer oxide, and already documented by the subtle *Amam* vs $Fmmm$ low-energy difference, the electronic states near the Fermi level are delicate. To reach a better understanding of the relevant coherence scales, we therefore performed additional calculations at higher T. Figure 2 shows that the low-energy regime reacts sensitively to temperature. The total spectral function [top panel of Fig. 2(a)] evolves from a QP-like structure at room temperature to a flattened weight around the Fermi level at $T = 80$ K. On the local level [middle panel of Fig. 2(a)], it is first noted that Ni-d_{z^2} and Ni-$d_{x^2-y^2}$ are both half filled. Second, upon lowering T, the near-ε_F $A_{loc}(\omega)$ transforms from QP-like, to a pseudogap, and finally to a low-amplitude peak. A link between the total and local spectrum may be established via the hybridization function $-\mathrm{Im}\,\Delta_h$, shown in the bottom panel of Fig. 2(a). It displays a (pseudo)gap at $T = 80$ K, altogether rendering it obvious that a NFL state is reached. The Ni-e_g self-energies shown in Fig. 2(b) underline this picture with a low-frequency upturn at low T. A Fermi-liquid (FL) fit to the room-T data yields effective masses $m^*_{z^2} = 6.4$ and $m^*_{x^2-y^2} =$ 5.6. But note that even the ambient system is not a good FL. Though a linear-in-frequency regime holds for the smallest Matsubara ω_n, the scattering rate $\sim -\lim_{\omega_n \to 0} \Sigma(i\omega_n)$ remains quite large for the given T, and already the $T = 150$ K

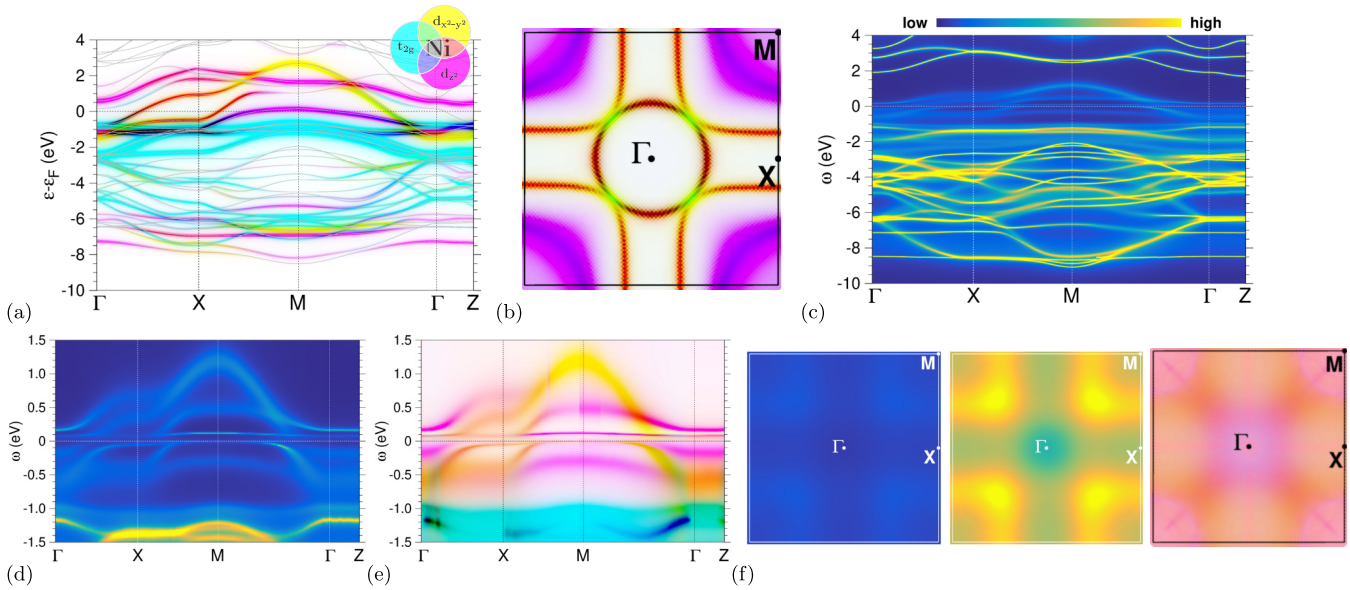

FIG. 3. **k**-dependent spectral features of the $Fmmm$ phase from (a), (b) DFT and [(c)–(f)] DFT+sicDMFT at $T = 80$ K. (a) DFT band structure in Ni($3d$)-fatspec representation. Note that red, green, and purple colors correspond to mixed-orbital states according to the color-coding inset. (b) DFT $k_z = 0$ Fermi surface in Ni-fatspec representation. (c) Interacting spectral function in a large energy window, and (d) in a small window around ε_F. (e) Same as (d) but in Ni-fatspec representation. (f) Interacting $k_z = 0$ Fermi surface from left to right: regular intensity, 10× increased intensity, Ni-fatspec representation.

data display further NFL tendencies. Because of half-filled Ni-e_g (one electron in each of the two orbitals) as well as the very low-energy scale for non-QP formation, a sole U- or J_H-driven NFL behavior does not seem likely.

Let us thus turn to the **k**-resolved spectra to gain insight into the origin of the NFL behavior. Figures 3(a) and 3(b) display the DFT band structure and Fermi surface to set the stage. The Ni-fatspec representation [62] marks the dominant Ni($3d$) character, showing that there are majorly four Ni-e_g dispersions, associated with the two equivalent Ni sites in the unit cell, governing the low-energy region. The inner two bands form a (α) electron pocket around Γ and a (β) hole sheet opening towards X. Note that those two Fermi-surface sheets are strongly Ni-$d_{z^2}/d_{x^2-y^2}$ mixed. The upper (antibonding) Ni-d_{z^2}-dominated band, also having a sizable apical O($2p$) character, is not crossing ε_F. Instead, a self-doping mainly La-based band mingles into the Ni-e_g fourfold dispersion and gives rise to a large electron pocket around Z. Finally, the lower (bonding) Ni-d_{z^2}-dominated band forms flattened (γ) hole pockets around M. The Ni-t_{2g} character very weakly mixes into part of the Fermi-surface sheets, but otherwise has major weight below ε_F and does not play a key role for the low-energy physics.

With correlations at $T = 80$ K, i.e., deep into the NFL regime, the low-energy picture changes quite dramatically [see Figs. 3(c)–3(f)]. First, the near-ε_F dispersions become generally very weak in intensity. Figure 3(d) shows that while the dispersions *away* from the Fermi level still keep some renormalized coherence, *right at* ε_F they dissolve. This is orthogonal to the understanding of a FL state and marks the strong NFL nature of the pressurized bilayer system. Accordingly, the (weakly k_z-dependent) interacting Fermi surface displayed in Fig. 3(f) becomes very weak and blurry. Only when raising the representation intensity [the middle part of Fig. 3(f)] does a holelike "sheet" structure around M emerge. It is reminiscent of the original DFT Ni-d_{z^2} flat-band-based γ sheet, but with a stronger mixed Ni-e_g character [cf. right part of Fig. 3(f)]. The enhanced intermixing presumably comes from a correlation-induced meet-up with the Ni-$d_{x^2-y^2}$ branded β sheet in the Γ-M direction. This is also supported from the disappearance of the self-doping Z pocket from the Fermi surface. Such strong correlation-induced shifts of self-doping bands have already been observed in other nickelates [33,62,63]. It becomes intuitively obvious that all these very-low-energy ramifications in the interacting regime have to strongly build up on the present flat-band scenario. There, the introduced renormalizations create a large phase space for intriguing quantum fluctuations, rendering robust QP formation impossible [64–66].

Albeit the NFL character may be relevant for superconductivity, let us get a handle on SC instabilities from a weak-coupling perspective for coherent Fermi-surface sheets and leave the discussion of the role of the NFL behavior and its relevance for superconductivity to future studies. To do this, we constructed a 4×4 maximally localized Wannier [67] Hamiltonian for the Ni-e_g based DFT bands. It carries hopping integrals $t_{ij}^{\ell\ell'}$ for $\ell, \ell' = 1d_{z^2}, 1d_{x^2-y^2}, 2d_{z^2}, 2d_{x^2-y^2}$ and lattice sites i, j. Here, 1 and 2 refer to the two Ni sublattices in the $Fmmm$ structure. Adding local Coulomb interactions, the effective Hamiltonian reads

$$H = \sum_{i \neq j, \ell\ell', \sigma} t_{ij}^{\ell\ell'} c_{i\ell\sigma}^{\dagger} c_{j\ell'\sigma} + \sum_{i} \left(H_{\text{int}}^{(i)} + H_{\text{orb}}^{(i)} \right). \quad (1)$$

The on-site interaction $H_{\text{int}}^{(i)}$ has a Slater-Kanamori form, i.e., includes density-density terms as well as pair-hopping and spin-flip terms, parametrized by $\bar{U}$ and $\bar{J}_H$ (here given in units of the tight-binding bandwidth). Note that within the

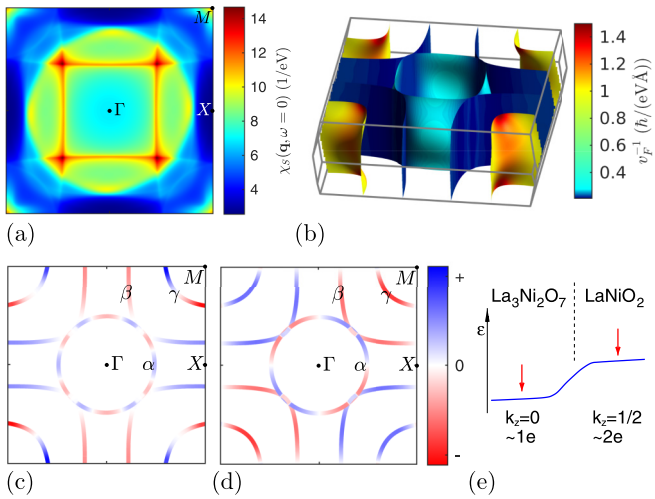

FIG. 4. (a) RPA spin susceptibility $\chi_S(\mathbf{q}, \omega = 0)$ for $\bar{U} = 0.36$ and $\bar{J}_H = \bar{U}/7$ at $T = 80$ K. (b) Absolute value of the inverse Fermi-surface velocity, showing significant anisotropy. (c), (d) Leading B_{1g} and B_{2g} solutions of the linearized gap equation for the same $\bar{U}$ and T as in (a) and $\bar{J}_H = \bar{U}/4$ and $\bar{J}_H = \bar{U}/7$, respectively. (e) Sketch for hole doping (red arrows) near the SC regime, relating flat-band scenarios of pressurized bilayer and reduced nickelates (see text).

downfolded model, the Hubbard interaction is screened more strongly, resulting in a smaller value than in the comprehensive DFT+sicDMFT treatment. The remaining noninteracting on-site $H^{(i)}_{\text{orb}}$ carries crystal-field terms via on-site levels ε_ℓ. In order to investigate the pairing symmetry starting from the effective band structure, we employ the standard multiorbital RPA treatment, developed by Graser *et al.* [68], to derive a linearized gap equation. This treatment is, i.e., a pertubative weak-coupling expansion in the Hubbard-Kanamori-type interaction and provides reliable insight into the leading pairing instabilities in layered unconventional superconductors, including nickelates [26]. Further details are presented in the Supplemental Material [53]. We calculate the RPA spin (charge) susceptibility $\chi_S(\mathbf{q}, \omega = 0)$ (χ_C) based on a two-dimensional cut through the first and second Brillouin zone to include relevant scatterings between the $k_z = 0$ and $k_z = 1/2$ layers. Figure 4(a) shows the obtained peak structure at $T = 80$ K, which is similar to previous findings [58]. The inverse of the band velocities $\mathbf{v}^\mu_F = \hbar^{-1}\nabla_{\mathbf{k}}\epsilon^\mu_{\mathbf{k}}$ at the Fermi surface is illustrated in Fig. 4(b). Here, $\epsilon^\mu_{\mathbf{k}}$ is the μth eigenvalue of the noninteracting Hamiltonian. The anisotropy of the band velocities proves relevant when solving the linearized gap equation. For $\bar{J}_H = \bar{U}/4$ the B_{1g} solution depicted in Fig. 4(c) is the leading solution. When the Hund exchange is weaker, the B_{2g} solution is leading. It is shown in Fig. 4(d) for $\bar{J}_H = \bar{U}/7$. A subleading $s_\pm$-wave solution, which belongs to the A_{1g} irreducible representation, becomes dominant when alterations to the band structure either reduce the anisotropy of the inverse band velocity on the z^2-dominated γ sheet near the M point, and/or when the van Hove singularity at the X shifts closer to the Fermi surface. This shift effectively also increases the inverse of the Fermi velocity of the β sheet. A more detailed discussion of the distinct solutions and their dependency on the details of the band structure is presented in the Supplemental Material [53], using the tight-binding model by Luo *et al.* [58] as an additional illustration. The total pairing strength given by the leading eigenvalue is strongly driven by $\bar{U}$, and generally, superconductivity would sensitively react to the level of of Ni-$d_{x^2-y^2}/d_{z^2}$ incoherence. This issue should be a subject of further theoretical and experimental study. Let us reiterate that the present RPA study of the superconducting instability is not perfectly adequate for the uncovered NFL normal state, but a reasoning can be given as follows. First, the Ni-e_g renormalizations in the (near) FL state at higher T are only weakly orbital dependent and therefore the Fermi surface of a highly renormalized FL approximant to the NFL state is expected to resemble the LDA picture. Second, the NFL Fermi surface just singles out the γ sheet, which is indeed most relevant for superconductivity in our RPA analysis.

Discussion. We have shown that the peculiar correlated electronic structure and concomitant SC instability of $La_3Ni_2O_7$ originates from the interplay of half-filled Ni-e_g orbitals within a Ni-d_{z^2}-created flat-band scenario. The role of O($2p$) is enhanced compared to reduced nickelates, yet a decisive role cannot be deduced from this initial theory study. But note that the Ni-O distance along c within the bilayer turns out remarkably small, thus intersite Ni-Ni self-energies may not be negligible. Those could, e.g., be addressed in a two-site, two-orbital cluster-DMFT study, which, however, is beyond the present scope. Comparing to the phenomenology of reduced nickelates, a line can be drawn between these and the bilayer system as sketched in Fig. 4(e) for a modelized single-Ni unit-cell system: In the reduced systems, the hole doping relevant for superconductivity occurs mainly in the Ni-d_{z^2} upper-branch flat-band part around $k_z = 1/2$ [23,55], corresponding to a well-filled Ni-d_{z^2} orbital. For pressurized $La_3Ni_2O_7$, however, the hole doping takes place in the lower-branch flat-band part around $k_z = 0$. There, Ni-d_{z^2} is close to half filling, much more correlated and therefore more on par with Ni-$d_{x^2-y^2}$. This should be the reason for the different T_c in the unlike nickelates. One may speculate that this different flat-band doping regime can also be realized in reduced multilayer nickelates [7,62,69] via tailored doping protocols even at ambient pressure.

Acknowledgments. The work is supported by the German Research Foundation within the bilateral NSFC-DFG Project No. ER 463/14-1. Computations were performed at the Ruhr-University Bochum and the JUWELS Cluster of the Jülich Supercomputing Centre (JSC) under project miqs.

[1] H. Sun, M. Huo, X. Hu, J. Li, Z. Liu, Y. Han, L. Tang, Z. Mao, P. Yang, B. Wang, J. Cheng, D.-X. Yao, G.-M. Zhang, and M. Wang, Nature (London) **621**, 493 (2023).

[2] D. Li, K. Lee, B. Y. Wang, M. Osada, S. Crossley, H. R. Lee, Y. Cui, Y. Hikita, and H. Y. Hwang, Nature (London) **572**, 624 (2019).

[3] D. Li, B. Y. Wang, K. Lee, S. P. Harvey, M. Osada, B. H. Goodge, L. F. Kourkoutis, and H. Y. Hwang, Phys. Rev. Lett. **125**, 027001 (2020).

[4] S. Zeng, C. S. Tang, X. Yin, C. Li, M. Li, Z. Huang, J. Hu, W. Liu, G. J. Omar, H. Jani, Z. S. Lim, K. Han, D. Wan, P. Yang, S. J. Pennycook, A. T. S. Wee, and A. Ariando, Phys. Rev. Lett. **125**, 147003 (2020).

[5] M. Osada, B. Y. Wang, B. H. Goodge, K. Lee, H. Yoon, K. Sakuma, D. Li, M. Miura, L. F. Kourkoutis, and H. Y. Hwang, Nano Lett. **20**, 5735 (2020).

[6] M. Osada, B. Y. Wang, B. H. Goodge, S. P. Harvey, K. Lee, D. Li, L. F. Kourkoutis, and H. Y. Hwang, Adv. Mater. **33**, 2104083 (2021).

[7] G. A. Pan, D. F. Segedin, H. LaBollita, Q. Song, E. M. Nica, B. H. Goodge, A. T. Pierce, S. Doyle, S. Novakov, D. C. Carrizales, A. T. N'Diaye, P. Shafer, H. Paik, J. T. Heron, J. A. Mason, A. Yacoby, L. F. Kourkoutis, O. Erten, C. M. Brooks, A. S. Botana *et al.*, Nat. Mater. **21**, 160 (2022).

[8] S. Zeng, C. Li, L. E. Chow, Y. Cao, Z. Zhang, C. S. Tang, X. Yin, Z. S. Lim, J. Hu, P. Yang, and A. Ariando, Sci. Adv. **8**, eabl9927 (2022).

[9] X. Wu, D. Di Sante, T. Schwemmer, W. Hanke, H. Y. Hwang, S. Raghu, and R. Thomale, Phys. Rev. B **101**, 060504(R) (2020).

[10] G.-M. Zhang, Y.-F. Yang, and F.-C. Zhang, Phys. Rev. B **101**, 020501(R) (2020).

[11] J. Karp, A. S. Botana, M. R. Norman, H. Park, M. Zingl, and A. Millis, Phys. Rev. X **10**, 021061 (2020).

[12] I. Leonov, S. L. Skornyakov, and S. Y. Savrasov, Phys. Rev. B **101**, 241108(R) (2020).

[13] P. Adhikary, S. Bandyopadhyay, T. Das, I. Dasgupta, and T. Saha-Dasgupta, Phys. Rev. B **102**, 100501(R) (2020).

[14] M. Kitatani, L. Si, O. Janson, R. Arita, Z. Zhong, and K. Held, npj Quantum Mater. **5**, 59 (2020).

[15] E. Been, W.-S. Lee, H. Y. Hwang, Y. Cui, J. Zaanen, T. Devereaux, B. Moritz, and C. Jia, Phys. Rev. X **11**, 011050 (2021).

[16] B. Geisler and R. Pentcheva, Phys. Rev. Res. **3**, 013261 (2021).

[17] Y. Gu, S. Zhu, X. Wang, J. Hu, and H. Chen, Commun. Phys. **3**, 84 (2020).

[18] T. Plienbumrung, M. Daghofer, M. Schmid, and A. M. Oleś, Phys. Rev. B **106**, 134504 (2022).

[19] M. Jiang, M. Berciu, and G. A. Sawatzky, Phys. Rev. Lett. **124**, 207004 (2020).

[20] K. Held, L. Si, P. Worm, O. Janson, R. Arita, Z. Zhong, J. M. Tomczak, and M. Kitatani, Front. Phys. **9**, 810394 (2022).

[21] P. Werner and S. Hoshino, Phys. Rev. B **101**, 041104(R) (2020).

[22] F. Lechermann, Phys. Rev. B **101**, 081110(R) (2020).

[23] F. Lechermann, Phys. Rev. X **10**, 041002 (2020).

[24] F. Petocchi, V. Christiansson, F. Nilsson, F. Aryasetiawan, and P. Werner, Phys. Rev. X **10**, 041047 (2020).

[25] C.-J. Kang and G. Kotliar, Phys. Rev. Lett. **126**, 127401 (2021).

[26] A. Kreisel, B. M. Andersen, A. T. Rømer, I. M. Eremin, and F. Lechermann, Phys. Rev. Lett. **129**, 077002 (2022).

[27] A. Demourgues, F. Weill, B. Darriet, A. Wattiaux, J. Grenier, P. Gravereau, and M. Pouchard, J. Solid State Chem. **106**, 330 (1993).

[28] T. Mizokawa, D. I. Khomskii, and G. A. Sawatzky, Phys. Rev. B **61**, 11263 (2000).

[29] H. Park, A. J. Millis, and C. A. Marianetti, Phys. Rev. Lett. **109**, 156402 (2012).

[30] S. Johnston, A. Mukherjee, I. Elfimov, M. Berciu, and G. A. Sawatzky, Phys. Rev. Lett. **112**, 106404 (2014).

[31] A. Subedi, O. E. Peil, and A. Georges, Phys. Rev. B **91**, 075128 (2015).

[32] V. Bisogni, S. Catalano, R. J. Green, M. Gibert, R. Scherwitzl, Y. Huang, V. N. Strocov, P. Zubko, S. Balandeh, J.-M. Triscone, G. Sawatzky, and T. Schmitt, Nat. Commun. **7**, 13017 (2016).

[33] F. Lechermann, Electron. Struct. **4**, 015005 (2022).

[34] R. S. Perry, L. M. Galvin, S. A. Grigera, L. Capogna, A. J. Schofield, A. P. Mackenzie, M. Chiao, S. R. Julian, S. I. Ikeda, S. Nakatsuji, Y. Maeno, and C. Pfleiderer, Phys. Rev. Lett. **86**, 2661 (2001).

[35] R. A. Borzi, S. A. Grigera, J. Farrell, R. S. Perry, S. J. S. Lister, S. L. Lee, D. A. Tennant, Y. Maeno, and A. P. Mackenzie, Science **315**, 214 (2007).

[36] F. Lechermann, Q. Han, and A. J. Millis, Phys. Rev. Res. **2**, 033490 (2020).

[37] P. D. C. King, T. Takayama, A. Tamai, E. Rozbicki, S. M. Walker, M. Shi, L. Patthey, R. G. Moore, D. Lu, K. M. Shen, H. Takagi, and F. Baumberger, Phys. Rev. B **87**, 241106(R) (2013).

[38] Z. Zhang, M. Greenblatt, and J. Goodenough, J. Solid State Chem. **108**, 402 (1994).

[39] S. Taniguchi, T. Nishikawa, Y. Yasui, Y. Kobayashi, J. Takeda, S.-i. Shamoto, and M. Sato, J. Phys. Soc. Jpn. **64**, 1644 (1995).

[40] G. Wu, J. J. Neumeier, and M. F. Hundley, Phys. Rev. B **63**, 245120 (2001).

[41] D.-K. Seo, W. Liang, M.-H. Whangbo, Z. Zhang, and M. Greenblatt, Inorg. Chem. **35**, 6396 (1996).

[42] V. Pardo and W. E. Pickett, Phys. Rev. B **83**, 245128 (2011).

[43] F. Lechermann, W. Körner, D. F. Urban, and C. Elsässer, Phys. Rev. B **100**, 115125 (2019).

[44] D. Grieger, C. Piefke, O. E. Peil, and F. Lechermann, Phys. Rev. B **86**, 155121 (2012).

[45] W. Körner and C. Elsässer, Phys. Rev. B **81**, 085324 (2010).

[46] C. Elsässer, N. Takeuchi, K. M. Ho, C. T. Chan, P. Braun, and M. Fahnle, J. Phys.: Condens. Matter **2**, 4371 (1990).

[47] F. Lechermann, F. Welsch, C. Elsässer, C. Ederer, M. Fähnle, J. M. Sanchez, and B. Meyer, Phys. Rev. B **65**, 132104 (2002).

[48] B. Meyer, C. Elsässer, F. Lechermann, and M. Fähnle, FORTRAN 90 program for mixed-basis-pseudopotential calculations for crystals (Max-Planck-Institut für Metallforschung, Stuttgart, 1998) (unpublished).

[49] P. Werner, A. Comanac, L. de' Medici, M. Troyer, and A. J. Millis, Phys. Rev. Lett. **97**, 076405 (2006).

[50] O. Parcollet, M. Ferrero, T. Ayral, H. Hafermann, I. Krivenko, L. Messio, and P. Seth, Comput. Phys. Commun. **196**, 398 (2015).

[51] P. Seth, I. Krivenko, M. Ferrero, and O. Parcollet, Comput. Phys. Commun. **200**, 274 (2016).

[52] B. Amadon, F. Lechermann, A. Georges, F. Jollet, T. O. Wehling, and A. I. Lichtenstein, Phys. Rev. B **77**, 205112 (2008).

[53] See Supplemental Material at http://link.aps.org/supplemental/10.1103/PhysRevB.108.L201121 for further details and additional data in view of the DFT, DFT+sicDMFT, and the RPA calculations, respectively.

[54] G. Kotliar, S. Y. Savrasov, K. Haule, V. S. Oudovenko, O. Parcollet, and C. A. Marianetti, Rev. Mod. Phys. **78**, 865 (2006).

[55] F. Lechermann, Phys. Rev. Mater. **5**, 044803 (2021).
[56] H. Chen, A. Hampel, J. Karp, F. Lechermann, and A. Millis, Front. Phys. **10**, 835942 (2022).
[57] V. I. Anisimov, I. V. Solovyev, M. A. Korotin, M. T. Czyżyk, and G. A. Sawatzky, Phys. Rev. B **48**, 16929 (1993).
[58] Z. Luo, X. Hu, M. Wang, W. Wú, and D.-X. Yao, Phys. Rev. Lett. **131**, 126001 (2023).
[59] M. Jarrell and J. E. Gubernatis, Phys. Rep. **269**, 133 (1996).
[60] H. J. Vidberg and J. W. Serene, J. Low Temp. Phys. **29**, 179 (1977).
[61] J. R. D'Errico, MATLAB Central File Exchange, https://de.mathworks.com/matlabcentral/fileexchange/34874-interparc (2012).
[62] F. Lechermann, Phys. Rev. B **105**, 155109 (2022).
[63] P. Worm, L. Si, M. Kitatani, R. Arita, J. M. Tomczak, and K. Held, Phys. Rev. Mater. **6**, L091801 (2022).
[64] S. Schmitt, Phys. Rev. B **82**, 155126 (2010).
[65] P. Kumar, T. I. Vanhala, and P. Törmä, Phys. Rev. B **100**, 125141 (2019).
[66] S. Sayyad, E. W. Huang, M. Kitatani, M.-S. Vaezi, Z. Nussinov, A. Vaezi, and H. Aoki, Phys. Rev. B **101**, 014501 (2020).
[67] N. Marzari, A. A. Mostofi, J. R. Yates, I. Souza, and D. Vanderbilt, Rev. Mod. Phys. **84**, 1419 (2012).
[68] S. Graser, T. A. Maier, P. J. Hirschfeld, and D. J. Scalapino, New J. Phys. **11**, 025016 (2009).
[69] J. Zhang, A. Botana, J. Freeland, D. Phelan, H. Zheng, V. Pardo, M. Norman, and J. F. Mitchell, Nat. Phys. **13**, 864 (2017).